Title

Low-loss tunable capacitors fabricated directly on gold bottom electrodes

Journal

Applied Physics Letters, 88

Author

Stemmer, Susanne

Publication Date

2006

DOI

10.1063/1.2186077

Peer reviewed

Low-loss tunable capacitors fabricated directly on gold bottom electrodes

Jiwei Lu[1], Steffen Schmidt[1], Damien S. Boesch[1], Nadia Pervez[2], Robert A. York[2] and Susanne Stemmer[1*]

[1]Materials Department, University of California, Santa Barbara, CA 93106-5050, USA

[2]Department of Electrical and Computer Engineering, University of California, Santa Barbara, CA 93106-9560, USA

[*] Email: stemmer@mrl.ucsb.edu

Abstract

At microwave frequencies, conductor losses due to the bottom electrode resistance severely limit the performance of metal-insulator-metal capacitors that employ tunable dielectric thin films. Here we demonstrate that a novel tunable dielectric, bismuth zinc niobate (BZN), can be integrated directly with low-resistivity Au bottom electrodes. The favorable crystallization kinetics of the BZN pyrochlore structure allowed for a low thermal budget process compatible with Au electrodes. BZN thin films on Au bottom electrodes showed very low dielectric loss tangents of ~ 0.0005 and high dielectric tunabilities of ~ 50%. The Au/BZN interface was abrupt and free of reaction phases. At high frequencies (>1 MHz) the total Au/BZN capacitor device loss was significantly reduced compared to capacitors with Pt bottom electrodes. The low device losses of Au/BZN capacitors revealed an additional, device geometry-dependent loss mechanism that contributed significantly to the device loss at high frequencies.

Dielectric thin films, such as ferroelectric (Ba,Sr)TiO_3 (BST), that have an electric field tunable dielectric constant have been extensively studied to replace GaAs based semiconductor varactors for low-cost, high performance tunable circuits operating at microwave frequencies. High dielectric tunabilities are most effectively achieved by using metal-insulator-metal (MIM) capacitor structures. At microwave frequencies the conductor losses from the bottom electrode are believed to dominate the total device loss [1-5]. Minimizing the conductor loss would not only improve device performance but also facilitate the interpretation of the measured device loss in terms of the dielectric loss, whose precise frequency dependence is often unknown [6].

To reduce the conductor losses, thick metal bottom electrodes with a low electrical resistivity are required. Most microwave capacitors employ Pt bottom electrodes because of their chemical stability and ability to withstand the high-temperatures and oxidizing conditions during dielectric deposition. More recently, W and Cu electrodes have been studied [7,8]. However, these electrodes oxidize and require processing of the dielectric under highly reducing conditions, which cause high leakage currents [9-13]. In many respects, Au would be the ideal electrode material. Au has a much lower electrical resistivity (~ 2 □□ cm) than Pt (~ 9.7 □□ cm) [14] and does not oxidize. However, the low melting temperature of Au (~ 1064 °C) and the high deposition temperatures required for perovskite ferroelectrics make integration difficult.

We have recently demonstrated that thin films of non-ferroelectric bismuth zinc niobate ($Bi_{1.5}Zn_{1.0}Nb_{1.5}O_7$ or BZN) have high dielectric tunabilities (~ 55%) and very low dielectric loss tangents (less than 0.0005) [15]. BZN has the cubic pyrochlore structure [16] and is a high-temperature-stable equilibrium phase in the ternary Bi_2O_3-ZnO-Nb_2O_5

system [17]. At microwave frequencies, BZN thin film MIM capacitor structures with Pt bottom electrodes show high device quality factors (Q) of greater than 100 up to 10 GHz [18], comparable to the best reported BST devices [5]. The device Q-factor contains contributions from the dielectric, the bottom electrode, and parasitics from the large pads used to probe the devices [18]. In this paper we show that BZN thin films with excellent dielectric properties can be integrated directly with Au bottom electrodes, allowing for improved device Q-factors at high frequencies.

~ 200 nm thick Au layers were deposited by electron beam evaporation on *c*-plane sapphire covered with ~ 3 nm thick Ti adhesion layers with no intentional heating of the substrate. X-ray diffraction (XRD) ϕ-scans showed that the Au films were mostly epitaxial (111) oriented (with a some {100} oriented grains). BZN films were grown by radio-frequency (rf) magnetron sputtering from a stoichiometric target using an Ar/O_2 sputter gas mixture and a substrate temperature of ~ 300 °C. The sputter parameters were described elsewhere [15]. A post-deposition rapid thermal anneal (RTA) was performed for 5 minutes in ultra-high-purity N_2 at 750 °C to crystallize the films. The ramp-up time was about 10 s and it took about ~ 5 min for the samples to reach room temperature after the RTA.

As-deposited BZN film were amorphous or nanocrystalline [19]. XRD θ-2θ scans after the RTA showed that the BZN films crystallized in the cubic pyrochlore structure and were (111) textured [Fig. 1 (a)]. No secondary phases were detected. Figure 1 (b) shows a cross-section transmission electron microscopy (TEM) image of the BZN thin film on Au after the RTA. The interface with the Au electrode was smooth and free of reaction layers, as was confirmed by the high-resolution TEM [Fig. 1 (c)]. The

BZN film was fully crystallized, despite the very short annealing time, consistent with findings by others [20]. The short crystallization times likely reflected the relatively low kinetic barrier against crystallization typical for pyrochlore oxides [21].

A schematic of the device structure for dielectric characterization is shown in Fig. 2(a). The device process has been reported in detail elsewhere [15]. The top contacts were 150 nm Au/100 nm Pt. Shorted devices with the same geometry but without the BZN film were fabricated on the same wafer. The dielectric properties were characterized with an impedance analyzer (Agilent model 4294A) connected to air coplanar probes (Cascade Microtech, Inc.) using a 500 mV oscillation voltage. The relative permittivity ε_r was calculated from the capacitance C, i.e. $\varepsilon_r = C \cdot t / \varepsilon_0 \cdot A$, where t was the BZN film thickness (determined by TEM), ε_0 the vacuum permittivity and A the capacitor area. The capacitor area was 1500 μm^2, unless stated otherwise, and the distance between the top contacts was 50 μm. The loss tangent was calculated from the measured device quality factor Q, i.e. $\tan\delta = Q^{-1}$. The relative tunability was defined as $(\varepsilon_{max} - \varepsilon_{min})/\varepsilon_{max}$, where ε_{min} is the minimum measured permittivity at the maximum applied field, and ε_{max} is the dielectric constant at zero bias.

Figure 3 (a) shows the Q-factor and permittivity of a ~200 nm thick BZN film on the Au bottom electrode. The Q-factor of a BZN film deposited on a 100 nm Pt bottom electrode is also shown for comparison. The BZN film on the Pt electrode was crystallized at 750 °C for 5 minutes in air, using a ramp rate of 10 °C/min so that the total annealing time was ~150 minutes. This process had been shown earlier to yield films with very low losses and high permittivities [15,18]. Figure 3(a) showed that the BZN film on Au had a very high permittivity of ~ 180, similar to that of bulk BZN [22,23] and

BZN films on Pt electrodes [15]. The inset shows the dielectric tunability for a ~ 165 nm thick BZN film at positive bias voltages, which was about 53%, similar to BZN films on Pt electrodes [15].

While the permittivity was independent of the measurement frequency [Fig. 3(a)], the *Q*-factor was strongly frequency dependent. The equivalent circuit shown in Fig. 2(b) has been used to explain the frequency dependence [4,24,25], where R_s, G_{DC} and G_{AC} represented the series resistance of the electrodes, the DC leakage due to free-electron conduction through the film and the loss of the dielectric, respectively. The total device loss ($1/Q_{total}$) then had three components, as described by the following equations [4,24,25]:

$$\frac{1}{Q_{total}} = \frac{1}{Q_{Leakage}} + \frac{1}{Q_{BZN}} + \frac{1}{Q_{Electrode}} \tag{1}$$

$$Q_{Leakage} = \frac{\omega C}{G_{DC}} \tag{2a}$$

$$Q_{Electrode} = \frac{1}{\omega R_S C} \tag{2b}$$

where ω is the measurement frequency. Consistent with this model, the *Q*-factor increased with frequency at low frequencies (dominated by $Q_{Leakage}$) and was approximately constant between ~ 10 kHz and ~ 1 MHz (dominated by the bulk dielectric loss). In this frequency range, BZN on both bottom electrodes showed a *Q*-factor of > 2000 or a loss tangent of ~0.0005 (accurately quantifying such high *Q*-factors was beyond the resolution of the measurement method). Therefore, despite the low thermal budget used to obtain crystalline BZN films, the dielectric loss at these frequencies was about one order of magnitude lower than the best reported BST thin films [3,26,27].

Above ~ 1 MHz, the device Q-factor decreased with frequency. This has been attributed to the third term in Eqn. (1), i.e. the series resistance associated with the ohmic loss in the contact electrodes and any interfacial ("contact") resistance. Consistent with this interpretation, the Q-factor showed a weaker frequency dependence for the Au bottom electrode, due to its lower series resistance. At 100 MHz (the upper frequency limit of the impedance analyzer), the Q-factor for Au devices was about 334, whereas for the Pt devices it was about 111, i.e. Au electrodes improved the Q-factor by more than 200.

To quantify the contributions from the bottom electrode loss, R_s was measured using shorted devices. The measured R_s values corresponded to an Au resistivity of ~ 4.08 □□ cm and a Pt resistivity of ~ 9.6 □□ cm, in reasonable agreement with the bulk resistivities. Equation 2(b) was used to estimate $Q_{Electrode}$, which was then removed from the data, using Eqn. (1). Figure 3(b) shows the experimental data after removal of R_s. For both electrodes the Q-factor increased and the difference between the Au and Pt capacitors decreased. This showed that the model correctly accounted for the contribution of the bottom electrode resistance to the high-frequency loss of the device.

The frequency dependence of the data in Figure 3(b) showed, however, that an additional series resistance term not due to conductor losses contributed significantly to the device Q at high frequencies. Measurements showed that this term was area dependent, with smaller devices showing higher Q (Fig. 4). Therefore, this loss contribution was not a bulk dielectric effect, as this would have yielded a Q-factor independent of the device geometry. One possible explanation was a tunneling resistance between the metal and interface and surface states in the dielectric [28]. Such a

contribution would not be removed using shorted devices and test devices with surface passivation layers will be explored.

In summary, we have shown that a novel, tunable, low-loss dielectric, pyrochlore bismuth zinc niobate, could be integrated directly on Au bottom electrodes. The process may also be of interest for other applications that require a low thermal budget and high-quality, high-permittivity dielectric films, such as dynamic random access memories and decoupling capacitors.

Acknowledgements

The authors thank the National Science Foundation (NSF-CCF 0507227 and NSF-DMR 0307914) for support of this research. This work made use of the UCSB Nanofabrication Facility, a part of the NSF-funded NNIN network.

References

1. K. Ikuta, Y. Umeda, and Y. Ishi, Jpn. J. Appl. Phys. Part 2 **34,** L1211 (1995).
2. D. C. Dube, J. Baborowski, P. Muralt, and N. Setter, Appl. Phys. Lett. **74,** 3546 (1999).
3. J. D. Baniecki, R. B. Laibowitz, T. M. Shaw, P. R. Duncombe, D. A. Neumayer, D. E. Kotecki, H. Shen, and Q. Y. Ma, Appl. Phys. Lett. **72,** 498 (1998).
4. A. Tombak, J.-P. Maria, F. Ayguavives, J. Zhang, G. T. Stauf, A. I. Kingon, and A. Mortazawi, IEEE Microwave & Wireless Compon. Lett. **12,** 3 (2002).
5. A. Vorobiev, P. Rundqvist, K. Khamchane, and S. Gevorgian, Appl. Phys. Lett. **83,** 3144 (2003).
6. A. K. Tagantsev, V. O. Sherman, K. F. Astafiev, J. Venkatesh, and N. Setter, J. Electroceram. **11,** 5 (2003).
7. B. Laughlin, J. Ihlefeld, and J.-P. Maria, J. Amer. Ceram. Soc. **88,** 2652 (2005).
8. J.-P. Maria, B. A. Boyette, A. I. Kingon, C. Ragaglia, and G. Stauf, J. Electroceram. **14,** 75 (2004).
9. T. Tamura, K. Takai, H. Noshiro, M. Kimura, S. Otani, and M. Yamada, Jap. J. Appl. Phys. Part 2 **33,** L1697 (1994).
10. R.-V. Wang and P. C. McIntyre, J. Appl. Phys. **94,** 1926 (2003).
11. Y. Fukuda, K. Numata, K. Aoki, A. Nishimura, G. Fujihashi, S. Okamura, S. Ando, and T. Tsukamoto, Jpn. J. Appl. Phys. Part 2 **37,** L453 (1998).
12. J. D. Baniecki, R. B. Laibowitz, T. M. Shaw, K. L. Saenger, P. R. Duncombe, C. Cabral, D. E. Kotecki, H. Shen, J. Lian, and Q. Y. Ma, J. Europ. Ceram. Soc. **19,** 1457 (1999).

13. J. W. Lu, S. Schmidt, Y.-W. Ok, S. P. Keane, and S. Stemmer, J. Appl. Phys. **98,** 054101 (2005).

14. J. Bass, in *Landolt-Börnstein - Group III Condensed Matter, Vol. 15A* (Springer Verlag, 1982), p. 5.

15. J. W. Lu and S. Stemmer, Appl. Phys. Lett. **83,** 2411 (2003).

16. I. Levin, T. G. Amos, J. C. Nino, T. A. Vanderah, C. A. Randall, and M. T. Lanagan, J. Solid State Chem. **168,** 69 (2002).

17. T. A. Vanderah, I. Levin, and M. W. Lufaso, Europ. J. Inorg. Chem. **2005,** 2895 (2005).

18. J. Park, J. W. Lu, S. Stemmer, and R. A. York, J. Appl. Phys. **97** (2005).

19. J. W. Lu, Z. Q. Chen, T. R. Taylor, and S. Stemmer, J. Vac. Sci. & Technol. A **21,** 1745 (2003).

20. R. L. Thayer, C. A. Randall, and S. Trolier-McKinstry, J. Appl. Phys. **94,** 1941 (2003).

21. C. G. Levi, Acta Mater. **46,** 787 (1998).

22. M. Valant and P. K. Davies, J. Mater. Sci. **34,** 5437 (1999).

23. X. Wang, H. Wang, and X. Yao, J. Amer. Ceram. Soc. **80,** 2745 (1997).

24. B. Acikel, Ph.D. Thesis, University of California Santa Barbara, 2002.

25. T. R. Taylor, P. J. Hansen, N. Pervez, B. Acikel, R. A. York, and J. S. Speck, J. Appl. Phys. **94,** 3390 (2003).

26. J. Im, O. Auciello, and S. K. Streiffer, Thin Solid Films **413,** 243 (2002).

27. S. M. Bilodeau, R. Carl, P. C. v. Buskirk, J. F. Roeder, C. Basceri, E. E. Lash, C. B. Parker, S. K. Streiffer, and A. I. Kingon, J. Korean Phys. Soc. **32,** S1591 (1998).

28. H. Rohdin, N. Moll, A. M. Bratkovsky, and C.-Y. Su, Phys. Rev. B **59,** 13102 (1999).

Figure Captions

Figure 1 (color online):

(a) X-ray θ-2θ scan of the BZN film on Au/sapphire showing Bragg peaks from the Au electrode, the BZN film and the sapphire substrate. The unlabeled peak at $2\theta \sim 26°$ may be an artifact from the substrate. (b) Cross-section bright field image of a BZN film on Au after the RTA, recorded approximately along $\langle 110 \rangle_{Au}$. The BZN film was polycrystalline with a columnar grain structure. (c) HRTEM image of the BZN/Au interface recorded along $\langle 110 \rangle_{Au}$ showing a smooth, atomically abrupt interface free of reaction layers.

Figure 2 (color online):

(a) Schematic of the parallel plate capacitor device for dielectric measurements using on-wafer RF probing. (b) Equivalent circuit of the device, where R_s denotes the series resistance due to electrodes and interfaces, G_{DC} the leakage due to mobile charges, G_{AC} the AC dielectric loss and C the BZN capacitance.

Figure 3 (color online):

(a) Device Q-factor and permittivity of a ~ 200 nm thick BZN film capacitor on 200 nm Au bottom electrode as a function of frequency. The device Q-factor of a BZN thin film capacitor on a 100 nm Pt bottom electrode with the same device geometry is also shown. The inset shows the dielectric tunability of an Au/BZN capacitor with a ~ 165 nm thick BZN film measured at 1 MHz at positive bias voltages. (b) Frequency dependence of the Q-factors for Au and Pt bottom electrode devices after the removal of the conductor loss.

The capacitor area was 30×50 μm^2 and the distance between the top contacts was 50 μm. The large scatter in the high *Q*-factor data is a limitation of impedance analyzer.

Figure 4 (color online):

Q-factors for Au/BZN capacitors as a function of frequency and device size. The device dimensions were 25×25 μm^2 and 45×45 μm^2, respectively. The conductor losses were removed using the series resistance of shorted devices.

Figure 1

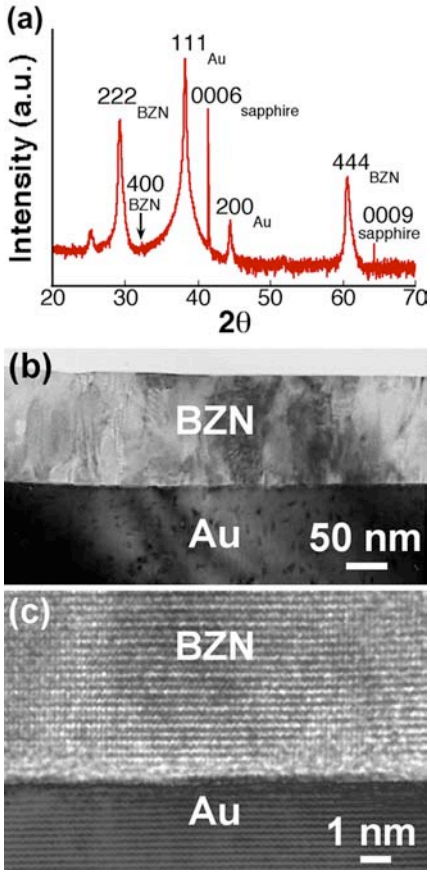
(a)
111 Au
222 BZN
0006 sapphire
444 BZN
400 BZN
200 Au
0009 sapphire
Intensity (a.u.)
20
30
40
50
60
70
2θ
(b)
BZN
Au
50 nm
(c)
BZN
Au
1 nm

Figure 2

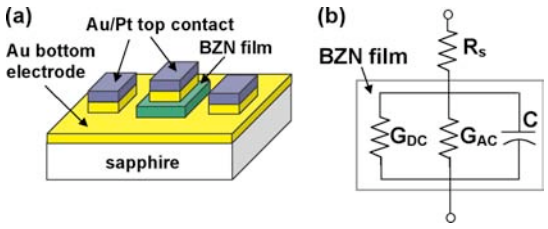
(a)
Au/Pt top contact
Au bottom electrode
BZN film
sapphire
(b)
BZN film
R_s
G_{DC}
G_{AC}
C

Figure 3

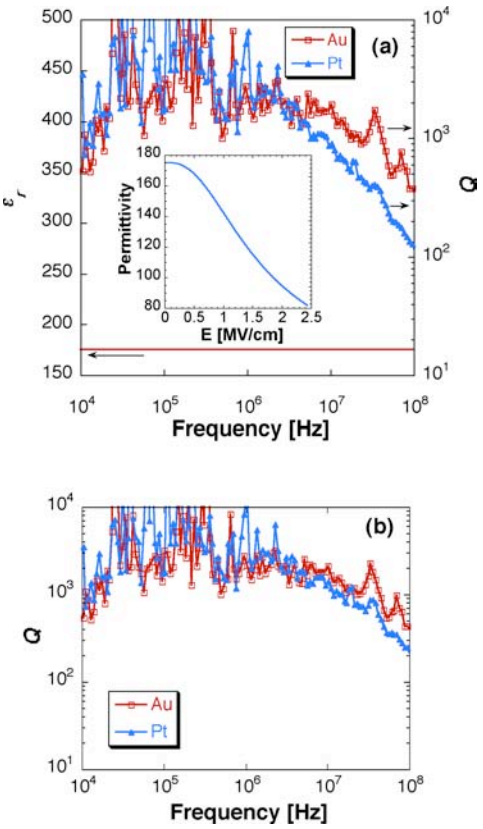
(a)
Au
Pt
ε_r
Q
Permittivity
E [MV/cm]
Frequency [Hz]
(b)
Au
Pt
Q
Frequency [Hz]

Figure 4

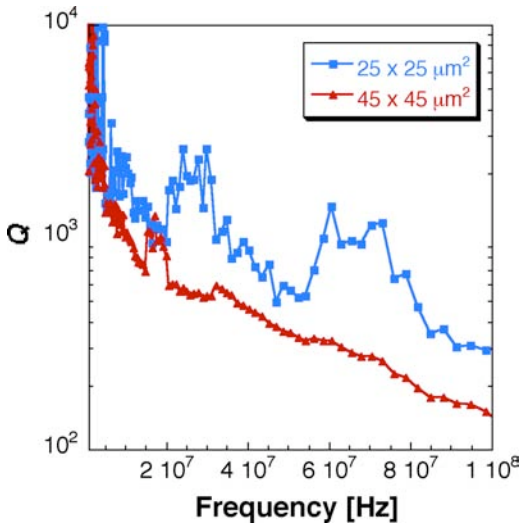
10^4
10^3
10^2
Q
25 x 25 μm²
45 x 45 μm²
2 10⁷
4 10⁷
6 10⁷
8 10⁷
1 10⁸
Frequency [Hz]